EnviKal-Loc: Sub-10m Indoor LoRaWAN Localization using an Environmental-Aware Path Loss and Adaptive RSSI Smoothing

Nahshon Mokua Obiri
University of Siegen
Siegen, Germany
nahshon.obiri@student.uni-siegen.de

Kristof Van Laerhoven
University of Siegen
Siegen, Germany
kvl@eti.uni-siegen.de

Abstract

LoRaWAN technology's extensive coverage positions it as a strong contender for large-scale IoT deployments. However, achieving sub-10 m accuracy in indoor localization remains challenging due to complex environmental conditions, multipath fading, and transient obstructions. This paper proposes a lightweight but robust approach combining adaptive filtering with an extended log-distance, multi-wall path loss and shadowing (PLS) model. Our methodology augments conventional models with critical LoRaWAN parameters (received signal strength indicator (RSSI), frequency, and signal-to-noise ratio (SNR)) and dynamic environmental indicators (temperature, humidity, carbon dioxide, particulate matter, and barometric pressure). An adaptive Kalman filter reduces RSSI fluctuations, isolating persistent trends from momentary noise. Using a six-month dataset of 1,328,334 field measurements, we evaluate three models: the baseline COST 231 multi-wall model (**MWM**), the baseline model augmented with environmental parameters (**MWM-EP**), and a forward-only adaptive Kalman-filtered RSSI version of the latter (**MWM-EP-KF**). Results confirm that the MWM-EP-KF achieves a mean absolute error (MAE) of 5.81 m, outperforming both the MWM-EP (10.56 m) and the baseline MWM framework (17.98 m). Environmental augmentation reduces systematic errors by 41.22%, while Kalman filtering significantly enhances robustness under high RSSI volatility by 42.63%, on average across all devices. These findings present an interpretable, efficient solution for precise indoor LoRaWAN localization in dynamically changing environments.

CCS Concepts

• **Networks → Wireless local area networks**; **Network performance modeling**.

Keywords

Indoor localization, Kalman filter, multiple linear regression, environmental parameters, path loss modeling

1 Introduction

The ability of LoRaWAN technology to deliver multi-kilometer connectivity with ultra-low power consumption has positioned it as a leading protocol for large-scale Internet of Things (IoT) deployments [6, 15]. While its physical layer (LoRa) excels in coverage, its utility for indoor localization, critical for applications like warehouse inventory tracking, hospital equipment monitoring, and smart factory workflows, remains constrained. The received signal strength indicator (RSSI)-based localization in LoRaWAN networks typically achieves 8–20 m accuracy [16], insufficient for fine-grained tracking where sub-10 m precision is required [10].

This limitation arises from signal attenuation dynamics unique to indoor environments, including multipath interference from reflective surfaces, absorption losses due to humidity fluctuations, and transient obstructions (e.g., personnel or equipment) [17, 22].

Traditional path loss models, such as the COST 231 multi-wall indoor attenuation model [5], approximate signal decay as a function of distance and static wall penetration losses. While these provide a foundational framework, they fail to account for dynamic environmental factors [2]. For instance, empirical studies demonstrate that temperature and humidity variations can alter the RSSI due to water vapor absorption at 868 MHz [4], [12]. At the same time, mobile obstacles like human beings subtly modify diffraction patterns [9]. Such effects introduce non-stationary noise that classical models treat as Gaussian shadowing, leading to systematic localization errors in real-world deployments.

Recent advances employ machine learning (ML) to map RSSI patterns to spatial coordinates. Random forests and convolutional neural networks (CNNs) achieve 5–7 m accuracy by learning complex relationships between RSSI, signal-to-noise ratio (SNR), and environmental variables [16], [20]. However, these models tend to operate as black boxes, obscuring the physical mechanisms driving signal attenuation. In safety-critical scenarios (e.g., tracking defibrillators in hospitals), the inability to diagnose why a model mislocates a device undermines trust and compliance. Furthermore, ML methods often require retraining when deployed in new environments, limiting scalability.

Our proposed work bridges these gaps by unifying physics-based propagation models with data-driven calibration. Building on the COST 231 Multi-Wall Model (**MWM**) framework [5], we extend the log-distance model to explicitly incorporate Environmental Parameter dynamics (temperature, relative humidity, carbon dioxide (CO_2), particulate matter ($PM_{2.5}$), and barometric pressure) and LoRa-specific parameters (RSSI, frequency, and SNR) (**MWM-EP**). Unlike many black-box-like ML models, our multiple linear regression (MLR) model quantifies the contribution of these factors. For example, by comparing the extended model with a baseline that only uses distance and wall-related parameters, we observed an improvement in R^2 from 0.6917 to 0.8222, indicating that the additional parameters explain approximately 13% more variance in path loss. This interpretability enables network operators to pinpoint attenuation sources (e.g., elevated $PM_{2.5}$ levels in a densely occupied indoor conference center degrading signals) and adjust deployments accordingly.

We deploy a per-device forward-only, innovation-based Kalman filter [11] on the MWM-EP to mitigate RSSI volatility as proposed in [13], resulting in the **MWM-EP-KF** formulation. It distinguishes transient noise, such as fleeting human movement, collisions, or

interference, from persistent path loss changes caused by environmental factors (heating, ventilation, and air conditioning), HVAC-induced temperature, and relative humidity shifts. Unlike traditional moving-average filters, which apply uniform weighting to all samples within a fixed window and introduce latency in dynamic environments, a Kalman filter dynamically tunes its process noise covariance based on real-time signal stability [3]. This adaptability enables precise separation of transient disturbances from sustained environmental shifts, a capability validated by recent advancements in adaptive filtering. For instance, hybrid frameworks like the Fourier-Transform Fuzzy-C-Means Kalman Filter (FFK) [19] demonstrate superior noise suppression in non-Gaussian RSSI distributions compared to static averaging methods, achieving 8% lower accumulated errors in dynamic indoor scenarios. Similarly, recursive Kalman-based approaches have proven robust against lag and outliers by prioritizing uncertainty-weighted updates over rigid windowed averaging[3].

The paper's contributions are threefold:

- (i) **Open Dataset and Analysis**: A public LoRaWAN dataset and analysis of LoRaWAN packets (with metadata) synchronized with environmental sensor readings, collected across seasons in a real-world office setting; available at: https://github.com/nahshonmokua/EnviKal-Loc.

- (ii) **Indoor Environmental-Aware Path Loss and Shadowing (PLS) Modeling**: A first-principles model augmented with environmental sensor data, achieving 5.81 m MAE in distance estimation. Coefficients for the MLR model parameters are derived from six months of indoor real-world office measurements

- (iii) **Self-Tuning Kalman Filter**: Device-specific, forward-only Kalman filter for adaptive RSSI smoothing that reduces localization volatility (σ from 9.95 dBm to 5.28 dBm) without prior noise statistics.

2 EnviKal-Loc: Design and Methodology

2.1 Data Collection Campaign

Our data measurement collection was conducted over a six-month indoor measurement campaign (mid-fall to mid-winter), using a single LoRaWAN gateway (GW) and six static end nodes (ENs). They were deployed in a typical office environment on the eighth floor (Figure. 1) of an academic building at the University of Siegen, Germany. This layout ensured a range of signal paths from unobstructed to heavily obstructed, emulating realistic indoor scenarios. The devices were distributed within a 40 m radius of the GW at a uniform height and placed to introduce varying propagation conditions. One EN-GW link was in line-of-sight (LoS), while others traversed multiple brick/concrete walls; non-line-of-sight (NLoS).

Each EN was housed in a custom 3D-printed enclosure with a vertically oriented omnidirectional antenna (Figure. 2) and incorporated a suite of co-located environmental sensors, including the Sensirion SCD41 for CO_2 concentration measurement, the Bosch BME280 for temperature, relative humidity, and barometric pressure levels, and the Sensirion SPS30 for $PM_{2.5}$ particulate concentration. The LoRaWAN nodes were built on Arduino MKR WAN 1310 boards, transmitting at 868 MHz with 20 dBm output power and adhering to the 1% duty cycle limit. Each device sent an 18 byte
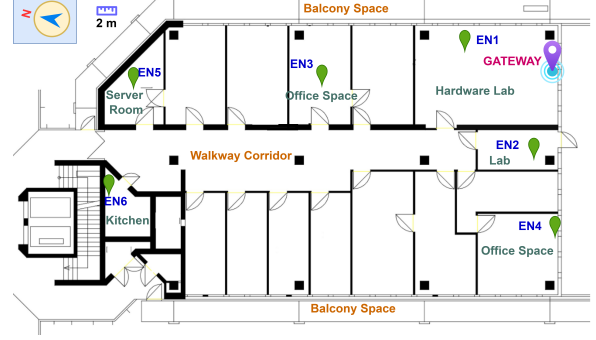

Figure 1: Sensor network deployment layout showing sensor end nodes (EN1–EN6) and the gateway (GW) placement.

uplink packet to the GW every 60 s, embedding sensor readings and a sequence counter in a compact binary format. To complete the network, a Kerlink Wirnet iFemtoCell indoor GW was configured for the EU868 band and provided robust indoor coverage with high receiver sensitivity (down to −141 dBm). It forwarded all received EN packets to a cloud-hosted network server (The Things Network), relaying the data via MQTT to an AWS-hosted InfluxDB time-series database.
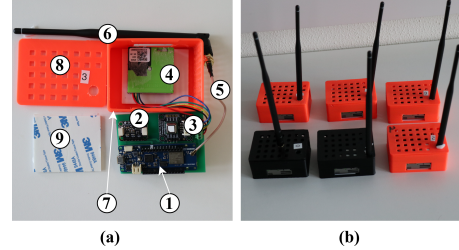

Figure 2: The end node: (a) Individual components: (1) Arduino MKR WAN 1310, (2) Adafruit BME280 sensor, (3) Sensirion SCD41 sensor, (4) Sensirion SPS30 sensor, (5) SMA to uFL adapter cable, (6) Rubber Duck antenna, (7) 3D-printed casing base, (8) 3D-printed casing lid, (9) mounting adhesive pads. (b) Fully assembled testbed end nodes.

Lastly, a continuously running Python script was deployed on an Amazon Web Services (AWS) EC2 instance to enable real-time, time-stamped logging of LoRaWAN link metrics (RSSI, SNR, spreading factor (SF), etc.) alongside environmental measurements. Each transmission's ground-truth parameters (known EN-GW distances, wall counts) were predetermined during deployment. To ensure data reliability, we implemented automated monitoring: a background script that polled the database and sent real-time alerts (via Telegram) if any device's data stream went silent (> 10 minutes), for timely intervention to minimize logging gaps.

2.2 Kalman Filtering for RSSI Refinement

RSSI volatility in indoor LoRaWAN links arises from transient obstructions (e.g., human movement) and environmental dynamics (e.g., HVAC-driven humidity shifts), which introduce non-Gaussian

noise. To address this, we deploy a lightweight, per-device self-tuning 1D Kalman filter, extending the innovation-driven framework of [13]. The filter uses a random-walk state and linear observation model to iteratively refine RSSI measurements, isolating persistent path loss trends from high-frequency fluctuations.

In Algorithm 1, RSSI is modeled as a slowly drifting random walk to represent realistic indoor conditions dominated by gradual environmental shifts (lines 4, 9–10). The process noise covariance ($Q = 0.003\,dB^2$, line 4) was heuristically selected based on pilot experiments [13], ensuring smooth tracking of genuine RSSI trends without responding excessively to transient noise (jitter). The initial measurement covariance ($R_0 = 0.22\,dB^2$, line 2) is significantly lower than the measured RSSI variance ($\sigma_z^2 \approx 9.95^2\,dB^2$), providing early-stage smoothing.

Measurement noise covariance (R_k) acts as a *gatekeeper*: adaptively updated via the innovation-driven approach, in which discrepancies between predicted and observed RSSI ("innovations") are exponentially smoothed and used to adjust the covariance in real time (lines 12–15). We use a long-memory factor ($\gamma = 0.99$, line 5) to gradually incorporate new conditions without abruptly forgetting past states. To avoid excessive sensitivity to short-lived outliers (adaptive noise rejection), the innovation ratio (α_k, line 12) is clipped between [0.95, 1.05] (line 13), and the measurement covariance (R_k) is clamped within [0.12, 0.38] dB^2 (line 15). This dynamic creates an adaptive noise-rejection threshold tailored to each device's micro-environment, ensuring stable filtering without confounding measurement and process uncertainties.

Algorithm 1 Self-Tuning 1D Kalman Filter for RSSI Refinement

Require: RSSI measurement sequence $\{z_k\}_{k=0}^{N-1}$
Ensure: Filtered RSSI estimates $\{\hat{x}_{k|k}\}_{k=0}^{N-1}$
    Initialization:
1: $\hat{x}_{0|0} \leftarrow z_0$ ▷ Initial state estimate
2: $P_{0|0} \leftarrow R_0$ ▷ Initial covariance ($R_0 = 0.22\,dB^2$)
3: $R \leftarrow R_0$ ▷ Initial measurement noise covariance
4: $Q \leftarrow 0.003\,dB^2$ ▷ Process noise covariance (fixed)
5: $\gamma \leftarrow 0.99$ ▷ Forgetting factor
6: $\alpha_{\min} \leftarrow 0.95, \ \alpha_{\max} \leftarrow 1.05$ ▷ Innovation bounds
7: $R_{\min} \leftarrow 0.12, \ R_{\max} \leftarrow 0.38\,dB^2$ ▷ Clamping range
8: **for** $k = 1, 2, \ldots, N-1$ **do**
    Prediction Phase:
9:     $\hat{x}_{k|k-1} \leftarrow \hat{x}_{k-1|k-1}$ ▷ State prediction
10:    $P_{k|k-1} \leftarrow P_{k-1|k-1} + Q$ ▷ Covariance prediction
    Innovation: ▷ Measures deviation from predicted RSSI
11:    $v_k \leftarrow z_k - \hat{x}_{k|k-1}$ ▷ Compute innovation
12:    $\alpha_k \leftarrow v_k^2/(P_{k|k-1} + R)$ ▷ Innovation ratio
13:    $\alpha_k \leftarrow \max(\alpha_{\min}, \min(\alpha_k, \alpha_{\max}))$ ▷ Clipping
    Noise Adaptation: ▷ Dynamic adjustment of noise covariance
14:    $R \leftarrow \gamma R + (1 - \gamma)\alpha_k R$ ▷ Exponential smoothing
15:    $R \leftarrow \max(R_{\min}, \min(R, R_{\max}))$ ▷ Covariance clamping
    Update Phase:
16:    $K_k \leftarrow P_{k|k-1}/(P_{k|k-1} + R)$ ▷ Kalman gain
17:    $\hat{x}_{k|k} \leftarrow \hat{x}_{k|k-1} + K_k v_k$ ▷ State update
18:    $P_{k|k} \leftarrow (1 - K_k)P_{k|k-1}$ ▷ Covariance update
19: **end for**

2.3 Environmental-Aware PLS Modeling

Natural variations in the office environment (occupant presence, HVAC activity, seasonal temperature/humidity shifts) contribute to dynamic changes during the measurements, providing a dataset to examine how transient factors affect signal propagation. The COST 231 multi-wall model (MWM), a classical log-distance PLS model, mainly accounts for distance and structural obstructions to express indoor PLS as given in Equation (1):

$$PLS = \beta + 10n \times \log_{10}\left(\frac{d}{d_0}\right) + \sum_{k=0}^{K} W_k L_k + \epsilon, \tag{1}$$

where β is the intercept (reference path loss at a 1 m distance, derived from free-space measurements), n is the path loss exponent due to distance, L_k is the fitted coefficient for a particular wall type (W_k) and ϵ represents random shadowing in indoor environments. We propose the MWM-EP model to enhance PLS prediction as a function of distance, frequency, environmental parameters, and SNR in Equation (2), as follows:

$$PLS = \beta + 10 \cdot n \cdot \log_{10}\left(\frac{d}{d_0}\right) + 20 \cdot \log_{10} f + \sum_{k=0}^{K} W_k \cdot L_k + \sum_{j=1}^{J} \theta_j \cdot E_j + k_s \cdot SNR + \epsilon, \tag{2}$$

where rationale behind the integration of each predictor in the model is as follows: *(i)* distance-dependent attenuation (n) models RSSI decay with distance according to a log-distance law characterized by a path loss exponent; *(ii)* the frequency term (f) introduces a frequency-dependent adjustment calibrated for the 868 MHz band, but generalizable to other LoRa frequencies if needed; *(iii)* wall penetration losses (W_k) represent attenuation from intervening walls, with distinct coefficients for different wall types (e.g., brick vs. wooden partitions); *(iv)* environmental factors (E_j) reflect how fluctuations in temperature, relative humidity, barometric pressure, $PM_{2.5}$, and CO_2 influence signal attenuation; *(v)* the signal quality indicator (SNR) captures channel impairments such as interference or noise-floor variations not explained by environmental factors; and *(vi)* stochastic shadowing (ϵ) accounts for unmodeled variability through a log-normal random term, preserving consistency with the observed RSSI variance.

Rather than assuming a theoretical free-space reference path loss, we empirically estimate β from our measurements. This approach captures constant factors (antenna gains, floor layout) in the model calibration, improving its realism for indoor conditions [2]. First, we preprocessed all collected data, eliminating duplicates and obvious outliers (e.g. repeated transmissions within 2 s via the network server acknowledgments). We use SFs 7–10 to balance range and throughput, ensuring indoor sensitivity without excessive airtime that skews modeling [14]. An Isolation Forest algorithm filtered spurious entries by examining anomalies in the multi-dimensional feature space (RSSI, SNR, environment) at a 1% contamination rate as recommended in [18].

We adopted a multivariate time-series causality analysis to determine how strongly environmental parameters predict indoor LoRaWAN RSSI fluctuations. Specifically, Vector Autoregression (VAR) with Granger causality tests was applied, selecting a lag order of 24 hours based on the Akaike Information Criterion (AIC = −5.906), using hourly-averaged data. The joint dynamics follow

the 7-dimensional VAR(24) process in Equation (3), using an hourly time index t:

$$\begin{bmatrix} RSSI_t \\ \mathbf{x}_t \end{bmatrix} = \mathbf{c} + \sum_{i=1}^{24} \mathbf{A}_i \begin{bmatrix} RSSI_{t-i} \\ \mathbf{x}_{t-i} \end{bmatrix} + \boldsymbol{\varepsilon}_t, \qquad \boldsymbol{\varepsilon}_t \sim \mathcal{N}(\mathbf{0}, \Sigma), \quad (3)$$

where $RSSI_t$ is the dependent and $\mathbf{x}_t = (CO_2, H, PM_{2.5}, P, T, SNR)^\top$ stacks the environmental parameters and SNR covariates. The intercept vector $\mathbf{c} \in \mathbb{R}^7$ represents baseline offsets, $\mathbf{A}_i$ are the lag-i coefficient matrices, and $\boldsymbol{\varepsilon}_t$ denotes zero-mean Gaussian innovations with covariance Σ. Causal directionality is evaluated via block-exogeneity (Granger) tests on the coefficient stack $\{\mathbf{A}_i\}_{i=1}^{24}$.

We then split the cleaned dataset into training (80%) and testing (20%) subsets as per [1]. Using the training portion, we fit the model parameters (n, L_k, θ_j, k_s) via least-squares regression to best match observed path loss. The model was then applied to the test data to predict path loss, and we computed standard errors (RMSE, R^2) and the standard deviation (ϵ). We also ran a 5-fold cross-validation to verify that our model maintained generalizability.

2.4 PLS-based Distance Estimation

Accurate distance estimation from RSSI measurements requires isolating the EN to GW distance d in the path loss model. For the MWM in Equation (1), we solve for the distance d by compensating for structural attenuation and log-normal shadowing:

$$d = d_0 \times 10^{\frac{PLS - \beta - \sum_{k=0}^{K} W_k L_k - \epsilon}{10n}}, \quad (4)$$

where $\epsilon \sim \mathcal{N}(0, \sigma^2)$ encapsulates shadow fading. In practice, ϵ is not directly observable, so it is commonly omitted ($\epsilon = 0$) during deterministic approaches, thus introducing an inherent margin of uncertainty. This practice aligns with recent work in [21] that treats shadowing as additive noise, favoring computational simplicity over strict statistical rigor. Also, simple experimental results in [20] show that neglecting ϵ can lead to inflated distance errors in NLoS settings.

The extended model (MWM-EP) in Equation (2) refines this by explicitly incorporating environmental and signal-quality terms. Solving for the distance d yields:

$$d = d_0 \times 10^{\frac{PLS - \beta - 20\log_{10} f - \sum_{k=0}^{K} W_k L_k - \sum_{j=1}^{P} \theta_j E_j - k_s SNR - \epsilon}{10n}}, \quad (5)$$

where, environmental parameters E_j and SNR reduce over-reliance on stochastic shadowing (ϵ) by capturing measurable variance. This approach balances systematic attenuation, such as humidity-induced absorption, and stochastic effects like transient human movement, ensuring robust indoor distance estimation.

The Kalman filter (Section 2.2) further mitigates ϵ's impact by smoothing RSSI measurements before inversion, effectively reducing σ^2 in our fitted model. This dual strategy of environmental compensation plus filtering yields more stable distance estimates than conventional model inversion, particularly in dynamic indoor settings where short-lived obstacles significantly affect shadowing.

3 Results and Discussion

We gathered 1,328,334 data samples covering a wide span of conditions. The VAR model Wald block-exogeneity tests confirmed that environmental and SNR drivers Granger-cause RSSI ($\chi^2_{144} =$

209.6, $p < 0.001$), while RSSI likewise Granger-causes the environmental block ($\chi^2_{144} = 306.0$, $p < 0.001$). These bidirectional links confirm that indoor LoRaWAN radio-link quality and micro-climate conditions form a tightly coupled system.

3.1 Kalman Filtering Performance

The Kalman filter reduces RSSI temporal volatility by 42.36% (from $\sigma = 9.95$ dB to $\sigma = 5.28$ dB) and mitigates error skewness from 3.725 to 0.622. This directly translates to stable localization: distance estimate RMSE drops by 61% (from 22.30 m to 8.70 m), crucial for sequential tracking in dynamic environments. As shown in (Figure. 3), filtered RSSI trajectories exhibit suppressed outliers (e.g., transient human obstruction on $t = $ 2024-12-20, corresponding to confirmed peak human occupancy (ground-truth) in the office during a team gathering) while preserving attenuation trends.
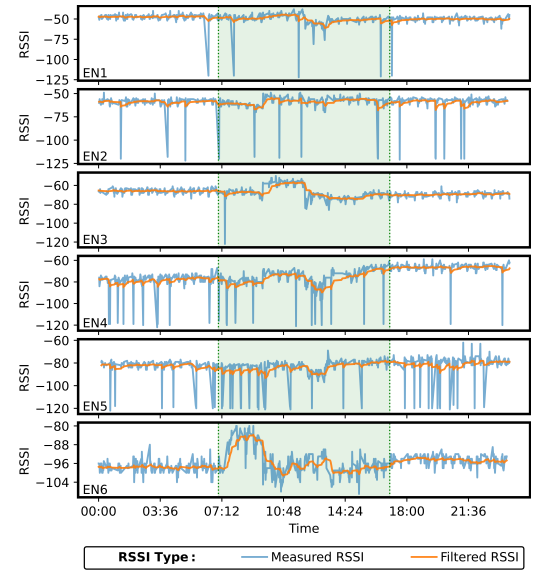

Figure 3: Kalman filter performance in smoothing RSSI fluctuations on 2024-12-20, with the shaded 07:00-17:00 interval marking confirmed peak occupancy.

3.2 Evaluation of PLS Modeling

The coefficient estimates in Table 1 reveal a complex interplay of environmental influences on indoor LoRaWAN propagation. Brick walls contribute +9.64 dB loss (vs.+2.62 dB for wood), aligning with the COST 231 MWM benchmarks but refined via empirical fitting. We obtain negative coefficients for the environmental parameters, contrary to outdoor study findings in [8]. This discrepancy often arises from unmodeled factors such as diurnal usage patterns or HVAC adjustments that temper absorption during high-humidity periods and subtle pressure-related operational shifts that incrementally affect path loss [7, 12]. For instance, HVAC-mediated compensation air circulation during high occupancy reduces vapor density, paradoxically improving signal penetration despite elevated CO_2. These relationships indirectly highlight how occupant behavior and atmospheric variables impact indoor wireless

channels. The SNR exhibits the most substantial impact on signal quality, which aligns with the novel classical propagation theory.

Table 1: MLR-estimated coefficients for the baseline (MWM) versus environment-augmented (MWM-EP, MWM-EP-KF) LoRaWAN indoor path-loss models.

Predictor (unit)	Model		
	MWM	**MWM-EP**	**MWM-EP-KF**
Reference path loss (**dB**)	31.301 024	5.462 682	−15.056 622
Path loss exponent (−)	3.618 965	3.195 524	3.563 895
Brick Wall loss (**dB**)	9.735 237	8.517 603	9.639 692
Wood Wall loss (**dB**)	2.638 829	2.981 828	2.619 658
CO_2 (**dB/ppm**)		−0.002 497	−0.003 955
Rel. humidity (**dB/%**)		−0.074 299	−0.108 241
$PM_{2.5}$ (**dB/(μg/m^3)**)		−0.153 206	−0.151 614
Bar. pressure (**dB/hPa**)		−0.011 567	0.000 412
Temperature (**dB/°C**)		−0.005 767	−0.084 215
SNR scaling factor (−)		−1.982 231	−0.355 351

Furthermore, applying a Kalman filter to the RSSI attenuates transient spikes, stabilizing the intercept (β), path loss exponent (n), and environmental coefficients so that sporadic interference no longer distorts model estimates. For example, the SNR scaling factor's magnitude (k_s) decreases substantially, and n remains anchored near its previously fitted value, indicating that noise-related outliers no longer overshadow genuine environment-driven changes. This yields a more consistent, physically interpretable framework for accurately estimating distances in indoor IoT deployments.

Residual analysis on the test dataset in (Figure. 4) confirms reduced noise in the filtered RSSI tight clusters near the ideal fit, contrasting raw data's diffuse spread (reduced RMSE) (see Figure. 5).
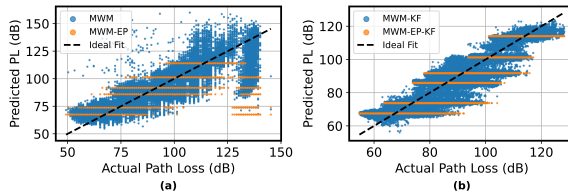

Figure 4: Comparison of predicted and actual path loss using the MWM and the MWM-EP models, with (a) the measured RSSI and (b) the filtered RSSI.

The extended baseline model (MWM-EP) reduces the test RMSE from 10.58 dB to 8.03 dB, a 24% improvement, due to the incorporation of environmental parameters. Due to Kalman filtering, the RMSE drops to 5.24 dB, halving the baseline MWM error. These gains align with prior evidence that humidity, CO_2, and other ambient factors explain a sizable portion of indoor RSSI variance once separated from random noise [12]. The filter's noise suppression also halves shadowing deviation (σ) and boosts model interpretability, enabling an $R^2 \approx 0.9020$. This combination outperforms purely data-driven or physics-based methods, blending the strengths of systematic environmental modeling with robust noise mitigation to improve localization reliability in indoor LoRaWAN deployments.
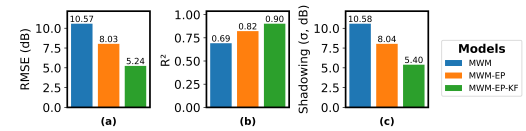

Figure 5: Evaluation of PLS fitting via: (a) RMSE, (b) coefficient of determination (R^2), and (c) shadowing standard deviation (σ) for the MWM, MWM-EP, and MWM-EP-KF models.

3.3 Distance Estimation Analysis

Precise indoor localization using LoRaWAN demands robust isolation of deterministic path loss from transient RSSI fluctuations. A hybrid approach coupling Kalman-filtered RSSI measurements with the MWM-EP model achieves superior distance estimation with an MAE of 5.81 m with a RMSE of 8.70 m (see Figure. 6). This significantly outperforms the conventional naïve single-gateway MWM (17.98 m MAE) and the MWM-EP (10.57 m MAE). Notably, incorporating environmental parameters mitigates systematic attenuation errors by 41.22%, explaining an additional RSSI variance previously only conflated with stochastic shadowing. Kalman filtering further reduces transient noise impact, significantly stabilizing RSSI measurements and aligning with recent adaptive filtering methodologies addressing non-Gaussian RSSI distributions [3].
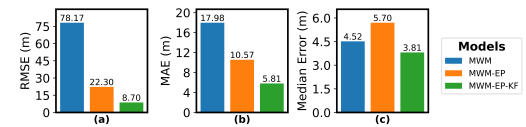

Figure 6: Comparison of distance estimation error across MWM, MWM-EP, and MWM-EP-FK models using: (a) RMSE, (b) MAE, and (c) Median Error.

Figure. 7 shows that the MWM-EP-KF framework consistently outperforms the other two approaches across diverse conditions. The baseline MWM yields a mean relative error of 24.41%, while simply adding environmental parameters (MWM-EP) increases it to 31.33% due to unfiltered sensor noise. Integrating Kalman filtering cuts this down to 21.13%, highlighting the synergy between environmental awareness and adaptive smoothing. Gains are particularly large in NLoS scenarios: EN3's error drops from 34.96% to 28.41%, and EN5's from 25.60% to 19.26%. Unlike black-box-like ML solutions [16], MWM-EP-KF remains interpretable and helps operators pinpoint specific attenuation sources, such as humidity or wall structures, for targeted optimization in real-world IoT deployments.
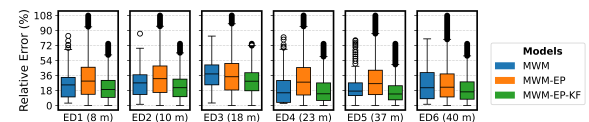

Figure 7: Relative error distributions per device for the MWM, the MWM-EP, and the MWM-EP-KF. Whiskers extend to $1.5 \times$ IQR, and outliers are shown as circles.

3.4 Study Limitations

Foremost, our dataset was collected in a single, typical academic office building, limiting immediate generalizability. Different architectural layouts, wall materials, and occupancy patterns in settings like warehouses, hospitals, and industrial plants can introduce different path loss and RSSI fluctuations. Additionally, our work assumes static end nodes, thus not capturing the complexities of mobile scenarios where frequent orientation changes and rapid environmental fluctuations may occur. Another constraint involves the reliance on accurate and timely sensor data: delays or inaccuracies in their measurements can degrade the system's performance. Moreover, we employed only one LoRaWAN gateway, which may not reflect the intricacies of multi-gateway deployments prone to coverage overlaps or synchronization issues. Finally, although the proposed Kalman filter substantially mitigates RSSI volatility, its empirically tuned parameters may require recalibration in environments with different interference levels or HVAC conditions.

4 Conclusion and Future Research Directions

This paper introduced the **MWM-EP-KF**, a method for indoor localization that combines physics-based, environment-aware path loss modeling with adaptive Kalman filtering optimized for LoRaWAN networks. Our experiments significantly improved distance estimation, achieving a mean absolute error of 5.81 m, notably outperforming conventional baseline approaches. By explicitly integrating environmental variables (relative humidity, CO_2, temperature, particulate matter ($PM_{2.5}$), and barometric pressure) into the path loss model, systematic errors were reduced by 41.22%. Concurrently, the Kalman filter effectively suppressed RSSI volatility, further enhancing accuracy and reliability. Therefore, our work bridges the gap between physics-based and data-driven localization by achieving accuracy previously reserved for resource-intensive ML.

Several research avenues remain open to advance this work. First, validating the proposed framework across diverse settings (e.g., industrial settings, healthcare facilities, and warehouses) will help evaluate its robustness with mobile nodes and scalability. Additionally, investigating nonlinear ML approaches (e.g., Extended/Unscented Kalman filters, reinforcement learning, neural networks) may enable continuous, automated calibration of model parameters in rapidly changing environments. Moreover, exploring multi-modal sensor fusion strategies (e.g., integrating occupancy detectors or BLE beacons) would enrich the dataset for advanced modeling. Lastly, extending our approach to multi-gateway deployments would address synchronization, distributed filtering, and large-scale data handling challenges. To support reproducibility and foster interpretable research, the relevant dataset and analysis scripts are available at https://github.com/nahshonmokua/EnviKal-Loc.

References

[1] Haider A. H. Alobaidy, Rosdiadee Nordin, Mandeep Jit Singh, Nor Fadzilah Abdullah, Azril Haniz, Kentaro Ishizu, Takeshi Matsumura, Fumihide Kojima, and Nordin Ramli. 2022. Low-Altitude-Platform-Based Airborne IoT Network (LAP-AIN) for Water Quality Monitoring in Harsh Tropical Environment. *IEEE Internet of Things Journal* 9, 20 (Oct. 2022), 20034–20054. https://doi.org/10.1109/JIOT.2022.3171294

[2] Joaquim Amândio Azevedo and Fábio Mendonça. 2024. A Critical Review of the Propagation Models Employed in LoRa Systems. *Sensors* 24, 12 (Jan. 2024), 3877. https://doi.org/10.3390/s24123877

[3] Wouter Bulten. 2015. Kalman Filters Explained: Removing Noise from RSSI Signals. https://www.wouterbulten.nl/posts/kalman-filters-explained-removing-noise-from-rssi-signals/.

[4] Marco Cattani, Carlo Alberto Boano, and Kay Römer. 2017. An Experimental Evaluation of the Reliability of LoRa Long-Range Low-Power Wireless Communication. *Journal of Sensor and Actuator Networks* 6, 2 (June 2017), 7. https://doi.org/10.3390/jsan6020007

[5] European Commission. 1999. *COST Action 231 - Digital Mobile Radio towards Future Generation Systems*. Final Report. European Commission, Directorate-General for the Information Society and Media, Luxembourg. 354 pages.

[6] Sezana Fahmida, Aakriti Jain, Venkata Prashant Modekurthy, Dali Ismail, and Abusayeed Saifullah. 2024. RTPL: A Real-Time Communication Protocol for LoRa Network. *ACM Trans. Embed. Comput. Syst.* 24, 1 (Dec. 2024), 17:1–17:31. https://doi.org/10.1145/3702209

[7] Zhaoji Fang, Hichem Guerboukha, Rabi Shrestha, Malachi Hornbuckle, Yasith Amarasinghe, and Daniel M. Mittleman. 2022. Secure Communication Channels Using Atmosphere-Limited Line-of-Sight Terahertz Links. *IEEE Transactions on Terahertz Science and Technology* 12, 4 (July 2022), 363–369. https://doi.org/10.1109/TTHZ.2022.3178870

[8] Mauricio González-Palacio, Diana Tobón-Vallejo, Lina M. Sepúlveda-Cano, Santiago Rúa, and Long Bao Le. 2023. Machine-Learning-Based Combined Path Loss and Shadowing Model in LoRaWAN for Energy Efficiency Enhancement. *IEEE Internet of Things Journal* 10, 12 (June 2023), 10725–10739. https://doi.org/10.1109/JIOT.2023.3239827

[9] Jascha Grübel, Tyler Thrash, Leonel Aguilar, Michal Gath-Morad, Didier Hélal, Robert W. Sumner, Christph Hölscher, and Victor R. Schinazi. 2022. Dense Indoor Sensor Networks: Towards Passively Sensing Human Presence with LoRaWAN. *Pervasive and Mobile Computing* 84 (Aug. 2022), 101640. https://doi.org/10.1016/j.pmcj.2022.101640

[10] Dongfang Guo, Chaojie Gu, Linshan Jiang, Wenjie Luo, and Rui Tan. 2022. ILLOC: In-Hall Localization with Standard LoRaWAN Uplink Frames. *Proc. ACM Interact. Mob. Wearable Ubiquitous Technol.* 6, 1 (March 2022), 13:1–13:26. https://doi.org/10.1145/3517245

[11] R. E. Kalman. 1960. A New Approach to Linear Filtering and Prediction Problems. *Journal of Basic Engineering* 82, 1 (March 1960), 35–45. https://doi.org/10.1115/1.3662552

[12] S. Lavdas, L. Zacharioudakis, A. Khalifeh, and Z. Zinonos. 2021. The Effect of Temperature and Humidity on Indoor LoRa Propagation Model. In *2021 17th International Conference on Distributed Computing in Sensor Systems (DCOSS)*. IEEE, Online, 374–379. https://doi.org/10.1109/DCOSS52077.2021.00066

[13] Tianrui Liao, Kaoru Hirota, Xiangdong Wu, Shuai Shao, and Yaping Dai. 2022. A Dynamic Self-Tuning Maximum Correntropy Kalman Filter for Wireless Sensors Networks Positioning Systems. *Remote Sensing* 14, 17 (Jan. 2022), 4345. https://doi.org/10.3390/rs14174345

[14] Wirlan G. Lima, Andreia V. R. Lopes, Caio M. M. Cardoso, Jasmine P. L. Araújo, Miércio C. A. Neto, Maria E. L. Tostes, Andréia A. Nascimento, Mauricio Rodriguez, and Fabrício J. B. Barros. 2024. LoRa Technology Propagation Models for IoT Network Planning in the Amazon Regions. *Sensors* 24, 5 (Jan. 2024), 1621. https://doi.org/10.3390/s24051621

[15] Nahshon Mokua Obiri and Kristof Van Laerhoven. 2024. A Survey of LoRaWAN-Integrated Wearable Sensor Networks for Human Activity Recognition: Applications, Challenges and Possible Solutions. *IEEE Open Journal of the Communications Society* 5 (2024), 6713–6735. https://doi.org/10.1109/OJCOMS.2024.3484002

[16] R. M. M. R. Rathnayake, Madduma Wellalage Pasan Maduranga, Valmik Tilwari, and Maheshi B. Dissanayake. 2023. RSSI and Machine Learning-Based Indoor Localization Systems for Smart Cities. *Eng* 4, 2 (June 2023), 1468–1494. https://doi.org/10.3390/eng4020085

[17] Nur Syazreen Ahmad. 2024. Recent Advances in WSN-Based Indoor Localization: A Systematic Review of Emerging Technologies, Methods, Challenges, and Trends. *IEEE Access* 12 (2024), 180674–180714. https://doi.org/10.1109/ACCESS.2024.3509516

[18] Jalaj Thanaki. 2018. *Machine Learning Solutions: Expert Techniques to Tackle Complex Machine Learning Problems Using Python* (1st edition ed.). Packt Publishing Ltd, Birmingham, UK.

[19] Chinyang Henry Tseng and Woei-Jiunn Tsaur. 2023. FFK: Fourier-Transform Fuzzy-c-means Kalman-Filter Based RSSI Filtering Mechanism for Indoor Positioning. *Sensors* 23, 19 (Jan. 2023), 8274. https://doi.org/10.3390/s23198274

[20] Hoang Vo, Van Hoang Long Nguyen, Van Lic Tran, Fabien Ferrero, Fang-Yi Lee, and Meng-Hsun Tsai. 2024. Advance Path Loss Model for Distance Estimation Using LoRaWAN Network's Received Signal Strength Indicator (RSSI). *IEEE Access* 12 (2024), 83205–83216. https://doi.org/10.1109/ACCESS.2024.3412849

[21] Yiting Wang, Jingqi Fu, and Yifan Cao. 2025. A Weighted Hybrid Indoor Positioning Method Based on Path Loss Exponent Estimation. *Ad Hoc Networks* 166 (Jan. 2025), 103684. https://doi.org/10.1016/j.adhoc.2024.103684

[22] Zhe Wei, Jialei Chen, Hai Tang, and Huan Zhang. 2024. RSSI-based Location Fingerprint Method for RFID Indoor Positioning: A Review. *Nondestructive Testing and Evaluation* 39, 1 (Jan. 2024), 3–31. https://doi.org/10.1080/10589759.2023.2253493